Analyst

PAPER

View Article Online
View Journal | View Issue

Cite this: *Analyst*, 2014, **139**, 3055

Acetylcholinesterase biosensor based on a gold nanoparticle–polypyrrole–reduced graphene oxide nanocomposite modified electrode for the amperometric detection of organophosphorus pesticides

Yuqi Yang,[a] Abdullah Mohamed Asiri,[b] Dan Du*[ac] and Yuehe Lin*[c]

Received 10th January 2014
Accepted 5th March 2014

DOI: 10.1039/c4an00068d

www.rsc.org/analyst

A nanohybrid of gold nanoparticles, polypyrrole, and reduced graphene oxide sheets (named as Au–PPy–rGO) was achieved by electrochemical deposition of reduced graphene oxide with pyrrole and the introduction of gold nanoparticles. Acetylcholinesterase (AChE) was further encapsulated in a silica matrix and immobilized on the Au–PPy–rGO nanocomposite by co-deposition with $(NH_4)_2SiF_6$. The presence of PPy helped to avoid the aggregation of rGO caused by van der Waals interactions between individual sheets and significantly increased the surface area of the modified electrode. The obtained Au–PPy–rGO nanocomposite not only showed excellent conductivity but also exhibited a high electrocatalytic activity and specific affinity for thiocholine, the hydrolysis product of the enzyme, and thus an improved detection sensitivity. Since AChE molecules were protected by the circumambient silica matrix, which provided a biocompatible environment and facilitated mass transport, the fabricated AChE biosensor displayed high stability and excellent activity together with a fast response to organophosphorus pesticides. Under optimum conditions, the biosensor led to the rapid and sensitive detection of paraoxon-ethyl from 1.0 nM to 5 μM with a detection limit of 0.5 nM.

1. Introduction

Organophosphates have been commercially used as pesticides, yet their contamination still remains a serious public concern for food safety and human health because of their long-term accumulation in the environment.[1] Although various analytical methods including chemiluminescence,[2] surface plasmon resonance,[3] chromatography,[4] mass spectrometry,[5] and piezoelectricity[6] have been developed to assess organophosphorus pesticide (OP) poisoning, their applications under field conditions are limited. The sustained prevalence of pollution continues to motivate the development of new methods for the detection of OPs in environmental and biological samples.

OPs are highly toxic because they can irreversibly inhibit the catalytic serine residue in cholinesterases (ChE) and subsequently prevent nerve transmission by blocking the breakdown of the transmitter choline.[7] Based on this principle, numerous inhibition biosensors have been developed for the detection of OPs.[8–10] However, during the fabrication of electrochemical enzyme biosensors, there are three main challenges: (1) providing large surfaces for enzyme immobilization;[11] (2) preventing enzymes from leaking out of the surfaces;[12] (3) maintaining the enzymes' activities.[13,14]

Graphene and its derivatives have shown outstanding electrochemical properties due to their extraordinarily high electrical and thermal conductivities, large surface areas, and potentially low manufacturing costs.[15–17] However, they usually suffer from serious aggregation caused by van der Waals interactions between individual sheets, resulting in relatively low active areas.[18] To solve this problem, other types of nanomaterials have been used together with graphene and various graphene-based hybrid materials have been reported.[8,19–21] Since graphene consists of sp^2-bonded carbon atoms with easily functionalized six-atom rings, and graphene oxide is abundant in reactive oxygen-containing groups,[22–24] other functional groups and other nanomaterials have been easily linked to graphene's surface.

In this paper, sulfonated reduced graphene oxide (rGO) was co-deposited with pyrrole by electrochemical scans. Due to strong chemisorptions between polymers and carbon materials, rGO was readily incorporated into the polypyrrole (PPy) to avoid aggregation. Gold nanoparticles (Au) were subsequently electrodeposited onto the PPy–rGO surface (Scheme 1). The obtained Au–PPy–rGO nanocomposite not only provides a large

[a]*Key Laboratory of Pesticide and Chemical Biology of Ministry of Education, College of Chemistry, Central China Normal University, Wuhan 430079, PR China. E-mail: dan.du@mail.ccnu.edu.cn*

[b]*Chemistry Department, King Abdulaziz University, Jeddah-21589, Saudi Arabia*

[c]*School of Mechanical and Materials Engineering, Washington State University, Pullman, WA 99164, USA. E-mail: yuehe.lin@wsu.edu*

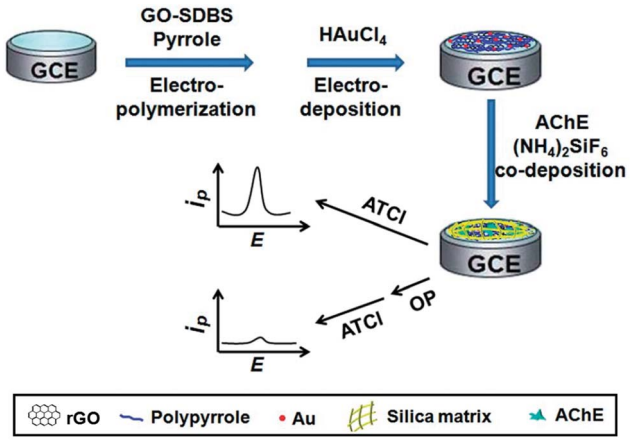

Scheme 1 Illustration of the preparation of the Au–PPy–rGO nanocomposite based AChE biosensor and its application for the electrochemical detection of organophosphorus pesticides.

and conductive platform for enzyme immobilization but also shows an excellent conductivity and strong affinity to the electro-active product, thiocholine. To avoid the desquamation and denaturation of the enzymes, acetylcholinesterase (AChE) was loaded by co-deposition with $(NH_4)_2SiF_6$. Results showed that the fabricated biosensor has great bioactivity and stability in a wide pH range.

2. Experimental

2.1 Reagents and apparatus

Acetylthiocholine chloride (ATCl) and AChE (Type C3389, 500 U mg^{-1} from electric eel) were purchased from Sigma-Aldrich (St. Louis, USA). Paraoxon-ethyl was obtained from Dr Ehrenstorfer GmbH (Augsburg, Germany). Graphite powder, sodium dodecylbenzenesulfonate (SDBS), hydrazine, pyrrole (98%), dodecylbenzene sulfonic acid (DBSA, >99%), $(NH_4)_2SiF_6$ and chloroauric acid ($AuCl_3 \cdot HCl \cdot 4H_2O$, 96%) were purchased from the Shanghai Chemical Reagent Co. (Shanghai, China), and used as received.

Electrochemical measurements were performed on a CHI660C workstation (Shanghai, China) with a conventional three-electrode system consisting of a platinum wire as the counter electrode, a saturated calomel reference electrode (SCE), and a glassy carbon electrode as the working electrode. Scanning electron microscopy (SEM) images were performed on a LEO 1450VP (Japan) scanning electron microscope. X-ray photoelectron spectroscopy (XPS) measurements were carried out with a thermoelectron instrument multilab 2000 (Thermo Fisher, USA).

2.2 Synthesis of rGO

Graphene oxide (GO) was prepared according to the modified Hummer's method[25] by the exfoliation of graphite. Typically, 38 mL concentrated H_2SO_4 was added to a mixture of 0.5 g graphite and 0.38 g $NaNO_3$ in a flask at 0 °C. Then, 0.23 g $KMnO_4$ was slowly added over about 1 h with stirring. After the mixture was kept stirring for 2 h in an ice-water bath and then stirred vigorously for 5 days at room temperature, 70 mL 5% H_2SO_4 aqueous solution was slowly added and kept stirring for another 2 h at 98 °C. Then, 1.5 mL of 30% H_2O_2 was added drop by drop, and the mixture was kept stirring for 2 h at room temperature. The resulting mixture was centrifuged and washed with a mixed solution of 3% H_2SO_4/0.5% H_2O_2, 3% HCl solution and water respectively to remove all of the metal ions and acid. Finally, the product was dried under vacuum.

Then, 10 mg of the above GO was dissolved in 100 mL water containing 0.01 M SDBS by ultrasonic treatment for 2 h. The color of the solution changed from yellow brown to black after GO was reduced with 30 μL hydrazine at 100 °C for over 24 h.[26] The resulting rGO–SDBS was separated centrifugally, washed with deionized water and dried under vacuum.

2.3 Fabrication of the AChE biosensor

Before modification, the glassy carbon electrode (GCE) was polished carefully with 1.0, 0.3, and 0.05 μm alumina slurries and sonicated for 3 min in nitric acid (v/v = 1 : 1). Before the experiment, a potential of +1.75 V was applied to the electrode for 300 s and then scanned from +0.3 V to +1.25 V and +0.3 V to +1.3 V until a steady-state current–voltage curve was obtained.

After being dried in N_2, the GCE was immersed into an aqueous solution containing 0.01 M DBSA, 0.05 M pyrrole, 1 mg mL^{-1} rGO–SDBS and protected with N_2 to prevent the oxidation and aggregation of the pyrrole. The deposition was performed by cyclic voltammetry (CV) from 0 to 1.0 V for 10 cycles. The resulting polypyrrole–rGO modified GCE (PPy–rGO/GCE) was washed with water and then transferred into 0.1% $HAuCl_4 \cdot 4H_2O$. An initial potential of −0.2 V was applied for 100 s to obtain Au–PPy–rGO/GCE.

Finally, the prepared Au–PPy–rGO/GCE was immersed into a NH_4Ac buffer containing 0.15 M $(NH_4)_2SiF_6$ and 50 U mL^{-1} AChE, with an applied constant cathodic current to accomplish the simultaneous deposition of the silica matrix and the AChE. The resulting biosensor (AChE/Au–PPy–rGO/GCE) was rinsed thoroughly with water and stored at 4 °C.

2.4 Electrochemical measurements

The obtained biosensor was immersed in PBS solutions containing different concentrations of paraoxon-ethyl for 15 min, and then transferred to an electrochemical cell of 1.0 mL pH 7.4 PBS containing 3.0 mM ATCl to test the electrochemical response. The inhibition was calculated as follows:

$$\text{Inhibition (\%)} = 100\% \times (i_{p,control} - i_{p,exp})/i_{p,control}$$

where $i_{p,control}$ and $i_{p,exp}$ were the peak currents of ATCl on AChE/Au–PPy–rCO/GCE without and with inhibition by paraoxon-ethyl, respectively.

3. Results and discussion

3.1 Electro-deposition of the Au–PPy–rGO nanocomposite

The rGO surface, which is abundant in dodecylbenzene sulfonic groups, was stable in a DBSA solution. During the

electropolymerization of pyrrole, negatively charged rGO sheets acting as a dopant, were readily incorporated into the polymer. Fig. 1 shows the CV responses of the electrodeposition on the GCE. One can see that a broad irreversible oxidation peak appeared at ~0.8 V in the first cycle and decreased quickly in the following cycles. Similar to the electropolymerization of pyrrole, the peak potential shifted to positive potentials in the continuous scans. Interestingly, the current dropped significantly in the first 3 cycles and was then enhanced in the following scans. This can be explained by the fact that the diffusion-limited oxidation of the pyrrole monomers might result in the decay of currents in the first three cycles. With the introduction of the rGO sheets, the amount of charge carrier increases. The resulting PPy–rGO/GCE was further loaded with Au nanoparticles by applying a negative potential of −0.2 V in 0.1% $HAuCl_4 \cdot 4H_2O$. The obtained Au–PPy–rGO nanocomposite not only increases the surface area but also enhances the surface conductivity. Moreover, Au nanoparticles have a strong affinity to thiocholine, which is the hydrolysis product of AChE, thus increasing the detection sensitivity.

The morphologies of PPy (A), PPy–rGO (B) and Au–PPy–rGO (C) were characterized by SEM, as shown in Fig. 2. The electrochemically polymerized polypyrrole displays compact and spherical particles, with a size distribution of 120–200 nm (Fig. 2A). However, when mixing rGO with pyrrole for the co-deposition, the obtained PPy–rGO, with a paper-like film, was totally different from PPy (Fig. 2B). It is easy to distinguish the edges of individual sheets as well as wrinkled areas. According to previous studies,[27,28] positively charged pyrrole monomers are first adsorbed onto the surface of the rGO–DBSA, and then electro-polymerized if a positive voltage is applied. After further decoration with Au nanoparticles, the formed Au–PPy–rGO nanocomposite clearly has an increased surface roughness. Uniform nanoparticles with a diameter of ~20 nm are dispersed homogeneously on the surface of the nanocomposite (Fig. 2C).

After encapsulating AChE in a three-dimensional porous silica matrix by electrochemical hydrolyzation of $(NH_4)_2SiF_6$, all of the relative areas are interconnected by small holes (Fig. 2D). Hydroxyl ions are produced near the electrode surface by the reduction of water in the electrodeposition process, which

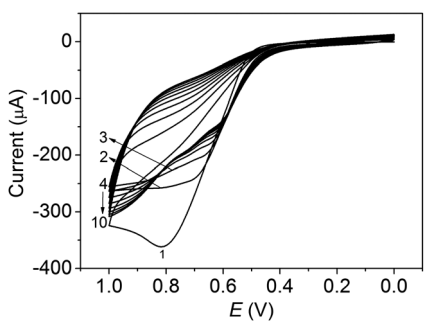

Fig. 1 Cyclic voltammograms of the electrochemical deposition process of 0.05 M pyrrole in solutions of 0.01 M DBSA and 1 mg mL^{-1} rGO–SDBS.

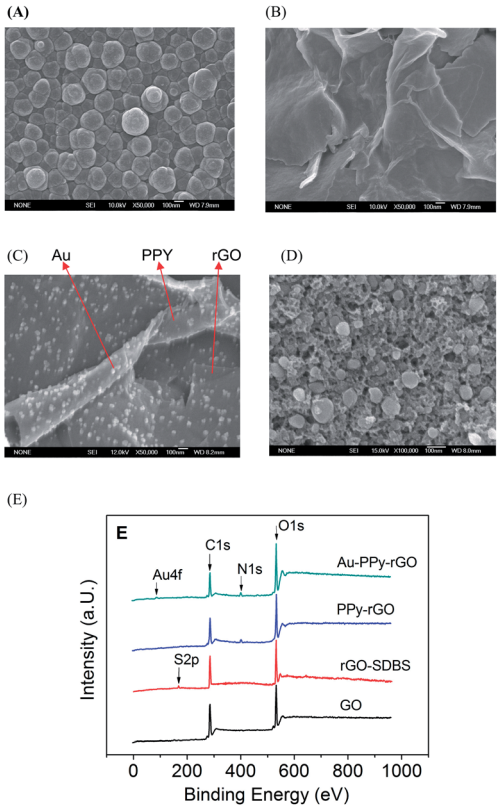

Fig. 2 SEM images of PPy (A), PPy–rGO (B), Au–PPy–rGO (C) and AChE on Au–PPy–rGO (D). PPy was prepared by electrochemical deposition of 0.05 M pyrrole in DBSA for 10 cycles. (E) XPS measurements of GO, rGO–SDBS, PPy–rGO, and Au–PPy–rGO.

catalyzes the hydrolysis of SiF_6^{2-} to $Si(OH)_4$ and eventually to the silica matrix.[29] On the other hand, hydrogen bubbles from the reduction of water circumscribe the silica to deposit along the gas/liquid interface and finally form the 3D porous structure. Meanwhile, AChE can be entrapped in the silica matrix simultaneously if it co-exists with the silica precursor electrolyte. We noticed that the presence of AChE did not change the 3D structure of the matrix.

X-ray photoelectron spectroscopy (XPS) measurements were further performed to analyze the composition of the prepared materials. As shown in Fig. 2E, all of the materials we prepared showed the same typical C 1s peaks at 284 eV and O 1s peaks at 532 eV. A new S 2p signal was observed for the rGO–SDBS composite, indicating that SDBS was successfully absorbed onto the rGO surface through π–π stacking interactions. A typical N1s peak was detected after the rGO–SDBS was electrodeposited onto the electrode surface with pyrrole, this confirmed the successful co-deposition of rGO with pyrrole. An additional component at 88 eV arose after the Au precursor was reduced on the PPy–rGO surface. These results indicate the formation of the Au–PPy–rGO composite.

3.2 Evaluation of the surface area

The electrochemical behaviors of Au–PPy–rGO and PPy–rGO were characterized by cyclic voltammetry (CV). As shown in

Fig. 3A, the GCE (curve a) and PPy–rGO/GCE (curve b) did not exhibit detectable peaks in PBS at applied potentials between 0 and 1.0 V. The background current becomes larger after the electrochemical polymerization of PPy–rGO on the GCE surface. This can be attributed to the favorable capacitance and conductivity of rGO. Two peaks appeared for Au–PPy–rGO/GCE (curve c), corresponding to the reduction reactions of Au(III)–Au(I) and Au(I)–Au(0),[9] which indicated that Au nanoparticles were successfully deposited on the surface of the PPy–rGO.

The electroactive areas were further investigated by $[Fe(CN)_6]^{3/4-}$ probe and estimated according to the Randles–Sevcik expression based on the slope of the different electrodes. As shown in Fig. 3B, the calculated surfaces of the GCE (curve a), PPy–rGO/GCE (curve b) and Au–PPy–rGO/GCE (curve c) were 0.15 cm^2, 1.28 cm^2, 1.66 cm^2, respectively. As expected, the rGO sheets and Au nanoparticles greatly increased the surface area, which is over 10 times higher than that of the bare electrode. Therefore, the Au–PPy–rGO/GCE is a good interface for enzyme immobilization.

3.3 Electrochemical behavior of AChE/Au–PPy–rCO/GCE

Fig. 4A shows the cyclic voltammetric curves of different AChE modified electrodes in the presence of 3.0 mM ATCl in pH 7.4 PBS. An irreversible peak at 0.64 V was observed for the AChE/GCE owing to the oxidation of the hydrolysis product of ATCl from catalysis of the immobilized AChE (curve a). When AChE was immobilized on the PPy–rGO/GCE, both the oxidation current and background increased obviously (curve b) compared to the bare GCE (curve a). It is due to the rGO, which possesses inherent conductive properties and a favorable capacitance. AChE was further electrodeposited on the Au/PPy–rGO/GCE. One can see that the peak current for the AChE/Au–PPy–rGO/GCE (curve c) was much higher than those for the AChE/PPy–rGO/GCE (curve b) and AChE/GCE (curve a). Since thiocholine displayed a very high oxidation potential on the bare electrode (~900 mV), the obtained Au–PPy–rCO/GCE based AChE biosensor makes the peak potential shift negatively to 680 mV. The over-potential decreases by 220 mV compared to that of the bare electrode, suggesting that the AChE/Au–PPy–rCO/GCE has a high

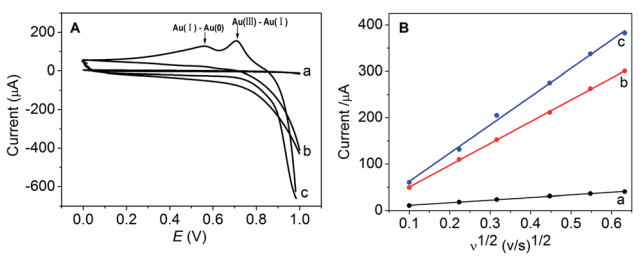

Fig. 3 (A) Cyclic voltammograms of the GCE (a), PPy–rGO/GCE (b) and Au–PPy–rGO/GCE (c) in 0.01 M PBS. (B) The relationship between the scan rates and the reduction peak currents of the $Fe(CN)_6^{4-/3-}$ probe (50 mM) on the GCE (a), PPy–rGO/GCE (b) and Au–PPy–rGO/GCE (c).

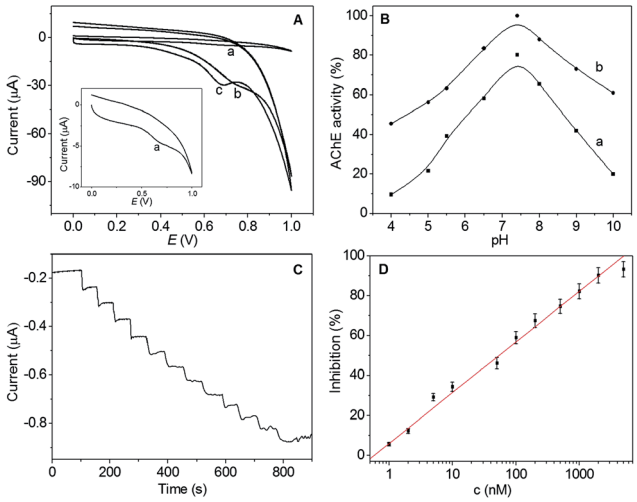

Fig. 4 (A) Cyclic voltammograms of 3 mM ATCl on AChE/GCE (a), AChE–PPy–rGO/GCE (b) and AChE/Au–PPy–rGO/GCE (c) in 0.01 M PBS (pH 7.4). (B) Effects of pH on the amperometric responses of the adsorbed AChE (a) and encapsulated AChE (b). The encapsulated AChE was achieved by electrolysis at 0.0118 A from 3.0 mL NH_4Ac buffer solution containing 0.15 M $(NH_4)_2SiF_6$ and 50 U mL^{-1} AChE HRP for 300 s on the Au–PPy–rGO/GCE. The adsorbed electrode was fabricated by the same procedure without AChE, and then coated with 3.0 μL AChE. (C) Amperometric current–time responses of the AChE/Au–PPy–rGO/GCE to ATCl. (D) Calibration curve of the AChE inhibition and paraoxon-ethyl concentrations.

electrocatalytic activity towards the oxidation of thiocholine. The improvement of the oxidation signal for the AChE biosensor results from the excellent conductivity of the Au nanoparticles and the rGO sheets. Furthermore, the specific affinity between the Au and mercapto groups makes the thiocholine easily concentrate on the electrode surface, thus increasing the detection response.

To ensure that the enzymes retained their bioactivities and conformations, AChE was encapsulated in a biocompatible silica matrix which could protect the AChE from being damaged by deleterious substances. It can be seen from Fig. 4B that both the adsorbed (curve a) and encapsulated (curve b) AChEs showed their highest activities in pH 7.4 PBS, while the activity of AChE improved a lot in acidic and alkaline surroundings after it had been encapsulated by a SiO_2 network. We assume that the encapsulated AChE molecules are surrounded by a silica matrix which prevents them from interacting with the outer environment.

Fig. 4C shows a typical steady-state current–time curve of electrochemical response *versus* successive addition of 0.1 mM ATCl at the working potential of 0.65 V. The electrochemical response increased as the concentration of ATCl increased. Most importantly, the current reached a stable value within 10 s after each addition, which showed that the electron-transfer was very fast and proved that the interconnected porous structure of the silica matrix did not prevent mass transport.

As a model of OPs, paraoxon-ethyl is known to be involved in the inhibition of AChE, and thus it reduces enzymatic activity.

The produced current for the AChE/Au–PPy–rGO/GCE decreases with the increase of paraoxon-ethyl concentration in solution. As shown in Fig. 4D, the inhibition increases with the concentration of paraoxon-ethyl from 1.0 nM to 5 μM with a detection limit of 0.5 nM.

The AChE activity based OP monitoring method was further validated with paraoxon-ethyl dosed tap water samples. Fresh tap water was solarized in the sun for 5 h, and then different amounts of paraoxon-ethyl were added to the water. Using the fabricated AChE/Au–PPy–rGO/GCE, we found that the inhibition of AChE increased with increasing OP concentration (Table 1). It is clear that the inhibition of AChE is directly related to paraoxon-ethyl exposure. These results indicate that the fabricated biosensor is reliable for detecting organophosphorus pesticides in practical samples.

The inhibited AChE can be reactivated by use of nucleophilic compounds such as pralidoxime iodide. Our group has successfully proved that an AChE based enzyme biosensor which is inhibited by OP compounds can retain 90% of its original activity after immersing it in 5.0 mM pralidoxime iodide.[30] Based on this reactivation procedure, the proposed biosensor could be used repeatedly with an acceptable reproducibility. When the enzyme electrode was not in use, it was stored at 4 °C in dry conditions. No obvious decrease in the response of ATCl was observed in the first 10 days. After a 30 day storage period, the sensor retained 90% of its initial current response.

4. Conclusion

In summary, we have developed an AChE biosensor based on a Au–PPy–rGO nanocomposite modified electrode for the rapid detection of OPs. The biosensor was prepared by subsequent mixing of pyrrole with reduced graphene oxide and $HAuCl_4$ for electro-deposition and further immobilization of AChE by co-deposition with $(NH_4)_2SiF_6$. Several advantages of the proposed method should be highlighted. (1) The obtained nanohybrid of Au–PPy–rGO not only increased the surface area of the modified electrode but also showed excellent conductivity. (2) AChE molecules were protected by a biocompatible 3D porous silica matrix to prevent them from leaking out and to retain their bioactivity. (3) The fabricated AChE biosensor displayed not only high stability and excellent activity but also a fast response to organophosphorus pesticides. This nanoassembly protocol is expected to be used for the immobilization of various enzymes and proteins, leading to robust biosensors.

Table 1 Detection of AChE activity in paraoxon-dosed tap water

Sample no.	1#	2#	3#	4#	5#	6#
Added OP (nM)	0	5	10	50	100	500
Determined inhibition (%)	<0.5	28.24	34.93	46.75	58.55	74.52
Standard inhibition (%)	0	29.36	34.11	45.84	60.09	76.83
Relative deviation (%)	—	−3.81	2.40	1.98	−2.56	−3.01

Acknowledgements

This work was supported by the National Natural Science Foundation of China (21275062) and the Program for New Century Excellent Talents in University (NCET-12-0871).

References

1 G. Scott, M. Fulton, D. Moore, E. Wirth, G. Chandler, P. Key, J. Daugomah, E. Strozier, J. Devane, J. Clark, M. Lewis, D. Finley, W. Ellenberg and K. Karnaky, *Toxicol. Ind. Health*, 1999, **15**, 200–213.
2 H. Y. Hu, X. Y. Liu, F. Jiang, X. Yao and X. C. Cui, *Chem. Cent. J.*, 2010, **4**, 13–18.
3 S. M. Daly, M. Grassi, D. K. Shenoy, F. Ugozzoli and E. Dalcanale, *J. Mater. Chem.*, 2007, **17**, 1809–1818.
4 A. G. Frenich, M. J. Gonzalez-Rodríguez, F. J. Arrebola and J. L. Martínez Vidal, *Anal. Chem.*, 2005, **77**, 4640–4648.
5 B. Hauser, M. Schellin and P. Popp, *Anal. Chem.*, 2004, **76**, 6029–6038.
6 G. G. Guilbault, J. Kristoff and D. Owens, *Anal. Chem.*, 1985, **57**, 1754–1756.
7 O. Lockridge, L. M. Schopfer and P. Masson, *Chapter 56 in Handbook of Toxicology of Chemical Warfare Agents*, ed. R. C. Gupta, Academic Press, 2009, pp. 847–858.
8 L. Zhang, A. Zhang, D. Du and Y. Lin, *Nanoscale*, 2012, **4**, 4674–4679.
9 D. Du, M. H. Wang, J. Cai, Y. H. Qin and A. D. Zhang, *Sens. Actuators, B*, 2010, **143**, 524–529.
10 (*a*) D. Du, S. Chen, D. Song, H. Li and X. Chen, *Biosens. Bioelectron.*, 2008, **24**, 475–479; (*b*) D. Du, X. Huang, J. Cai and A. D. Zhang, *Biosens. Bioelectron.*, 2007, **23**, 285–289.
11 Y. Teng, Y. Fu, L. Xu, B. Lin, Z. Wang, Z. Xu, L. Jin and W. Zhang, *J. Phys. Chem. B*, 2012, **116**, 11180–11186.
12 R. Solna, E. Dock, A. Christenson, M. Winther-Nielsen, C. Carlsson, J. Emneus, T. Ruzgas and P. Skladal, *Anal. Chim. Acta*, 2005, **528**, 9–19.
13 I. Gill and A. Ballesteros, *Trends Biotechnol.*, 2000, **18**, 282–296.
14 J. Zhang, F. Zhang, H. Yang, X. Huang, H. Liu, J. Zhang and S. Guo, *Langmuir*, 2010, **26**, 6083–6085.
15 D. A. C. Brownson, D. K. Kampouris and C. E. Banks, *Chem. Soc. Rev.*, 2012, **41**, 6944–6976.
16 D. A. C. Brownson and C. E. Banks, *Analyst*, 2010, **135**, 2768–2778.
17 Y. Y. Shao, J. Wang, H. Wu, J. Liu, I. A. Aksay and Y. H. Lin, *Electroanalysis*, 2010, **22**, 1027–1036.
18 Z. Cui, C. X. Guo, W. Yuan and C. M. Li, *Phys. Chem. Chem. Phys.*, 2012, **14**, 12823–12828.
19 Y. Li, W. Gao, L. Ci, C. Wang and P. M. Ajayan, *Carbon*, 2010, **48**, 1124–1130.
20 G. Williams, B. Seger and P. V. Kamat, *ACS Nano*, 2008, **2**, 1487–1491.
21 J. G. Radich and P. V. Kamat, *ACS Nano*, 2013, **7**, 5546–5557.
22 V. Georgakilas, M. Otyepka, A. B. Bourlinos, V. Chandra, N. Kim, K. C. Kemp, P. Hobza, R. Zboril and K. S. Kim, *Chem. Rev.*, 2012, **112**, 6156–6214.

23 D. Chen, H. Feng and J. Li, *Chem. Rev.*, 2012, **112**, 6027–6053.
24 X. Huang, X. Qi, F. Boey and H. Zhang, *Chem. Soc. Rev.*, 2012, **41**, 666–686.
25 H. A. Becerril, J. Mao, Z. Liu, R. M. Stoltenberg, Z. Bao and Y. Chen, *ACS Nano*, 2008, **2**, 463–470.
26 H. Chang, G. Wang, A. Yang, X. Tao, X. Liu, Y. Shen and Z. Zheng, *Adv. Funct. Mater.*, 2010, **20**, 2893–2902.
27 A. Liu, C. Li, H. Bai and G. Shi, *J. Phys. Chem. C*, 2010, **114**, 22783–22789.
28 P. V. Kamat, K. G. Thomas, S. Barazzouk, G. Girishkumar, K. Vinodgopal and D. Meisel, *J. Am. Chem. Soc.*, 2004, **126**, 10757–10762.
29 S. Yang, W. Z. Jia, Q. Y. Qian, Y. G. Zhou and H. Xia, *Anal. Chem.*, 2009, **81**, 3478–3484.
30 L. Zhang, L. Long, W. Zhang, D. Du and Y. Lin, *Electroanalysis*, 2012, **24**, 1745–1750.